

Robustness of topologically protected surface states in layering of Bi_2Te_3 thin films

Kyungwha Park, J. J. Heremans, V. W. Scarola, and Djordje Minic

Department of Physics, Virginia Tech, Blacksburg, Virginia 24061

(Dated: September 5, 2018)

Bulk Bi_2Te_3 is known to be a topological insulator. We investigate surface states of $\text{Bi}_2\text{Te}_3(111)$ thin films using density-functional theory including spin-orbit coupling. We construct a method to unambiguously identify surface states of thin film topological insulators. Applying this method for one to six quintuple layers of Bi_2Te_3 , we find that the topological nature of the surface states remains robust with the film thickness and that the films of three or more quintuple layers have topologically non-trivial or protected surface states, in agreement with recent experiments.

PACS numbers: 73.20.At, 73.20.-r, 71.20.Nr, 71.15.Mb

Recently, topological insulators (TIs) with time-reversal symmetry have attracted attention due to their topologically protected states [1–4]. In three dimensions, TIs differ from band insulators in that a bulk energy gap opens due to strong spin-orbit coupling (SOC) with metallic surface states in the bulk energy gap. Several bulk bismuth-based alloys were discovered to be three-dimensional TIs [2–13]. For ordinary metals, surface states are so fragile that they can be destroyed by a small number of impurities or disorder at the surface. However, the surface states of TIs are topologically protected in that impurities preserving time-reversal symmetry can neither destroy nor impact the topological nature of the surface states.

Three-dimensional TIs are classified according to a topological invariant, the Z_2 invariant ν_0 [1]. Strong (weak) TIs have $\nu_0 = 1$ ($\nu_0 = 0$). Recent first-principles calculations [5, 14] show that bulk Bi_2Te_3 , Bi_2Se_3 , and Sb_2Te_3 alloys are strong TIs with a single Dirac cone below the Fermi level, E_f , at Γ ($\vec{k} = 0$). This feature was confirmed by angle-resolved photoemission spectra (ARPES) experiments [4, 7–11].

Thin films offer valuable probes of TIs as well as potential device applications. It is, therefore, important to identify surface states and their topological properties. For example, thin TI films were proposed to be efficient thermoelectric devices that exploit the interaction between top and bottom surface states [15]. Thin films also have considerable advantages in a direct measurement of transport properties of the surface states by emphasizing surface states over bulk states. Very recently, Bi_2Te_3 and Bi_2Se_3 thin films with a thickness of a few nm were experimentally realized [16–20], and topological properties of such films have been examined [18–23]. One theory suggests that the quantum spin Hall phase of a thin TI film oscillates between topologically trivial ($\nu_0 = 0$) and non-trivial ($\nu_0 = 1$) states with the film thickness [21], while another study implies a topological quantum phase transition with an oscillation in an energy gap Δ with the thickness [23]. However, ARPES measurements [18–20] on thin films did not show any oscillation in either ν_0 or Δ with thickness. These discrepancies cast doubt on

the robustness of topological surface states and how to identify them.

In this work, we construct a method to unambiguously identify topologically protected surface states for thin TI films. Our method based on density-functional theory (DFT) with SOC, can be used to determine the topological nature of the surface states in thin TI films. As an example, we apply this method to Bi_2Te_3 thin films at six different thicknesses. We show that the topological nature of the surface states remains *robust* with the film thickness and that the surface states are topologically non-trivial ($\nu_0 = 1$) for films three or more quintuple layers (QLs) thick. This differs from previous calculations [21], yet agrees with experiment [19].

We begin with a review of the bulk properties of Bi_2Te_3 [24]. A unit cell of bulk Bi_2Te_3 consists of a rhombohedral structure with five inequivalent atoms: two Bi and three Te. For the lattice constants ($a=4.386$ Å and $c=30.497$ Å) and the positions of the five atoms, we use experimental data [25]. We calculate the electronic structure of bulk Bi_2Te_3 using a DFT code, VASP [26], within the Perdew-Burke-Ernzerhof (PBE) generalized-gradient approximation (GGA) [27]. Projector-augmented-wave (PAW) pseudopotentials are used [28]. Plane waves with a kinetic energy cutoff E_c of 175 eV are used as basis sets and 146 irreducible k -points ($N_k=146$) are sampled. Figure 1 shows the bulk band structure computed without and with SOC at time-reversal invariant momenta, Γ , Z , F , and L , with $E_f = 0$. At the Dirac point (Γ), SOC inverts the conduction and valence bands with opposite parities [5].

Let us discuss the structure of a $\text{Bi}_2\text{Te}_3(111)$ film and parameter values for band-structure calculations of the films. Along the (111) direction (trigonal axis), a Bi_2Te_3 slab is built in units of a QL, which consists of two Bi and three Te layers that alternate [inset in Fig. 2(b)]. In each atomic layer, the Bi or Te atoms form a triangular lattice, and their in-plane positions coincide with those in a (111) surface of a fcc lattice. For each QL [inset in Fig. 2(b)], the Te(1) and Bi(1)/Bi(2) layers bond more strongly than the Bi(1)/Bi(2) and Te(2) layers, since $z_1 < z_2$. Neighboring QLs are separated by

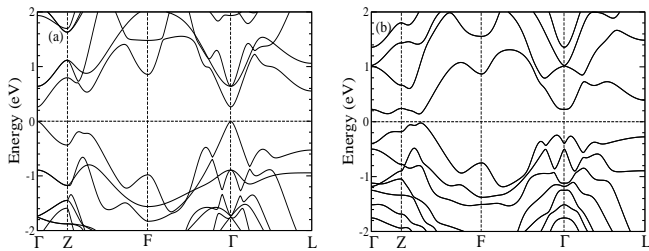


FIG. 1: Band structure of bulk Bi_2Te_3 (a) without SOC and (b) with SOC at symmetry points Γ , Z, F, and L.

TABLE I: The number of crossings N_c of the surface states across E_f , the energy gap Δ at $\bar{\Gamma}$, and the indirect energy gap ΔE_{ind} (eV) as a function of slab thickness (nm). E_c (eV) and N_k are the energy cutoff and the number of k points sampled, respectively.

no of QLs	thickness	E_c	N_k	Δ (eV)	N_c	ΔE_{ind}
1	1.0166	300	48	0.4338	0	0.301
2	2.0332	300	96	0.1319	0	0.057
3	3.0497	500	341	0.0261	1	No gap
4	4.0663	500	341	0.0070	1	No gap
5	5.0829	500	341	0.0090	1	No gap
6	6.0993	500	341	0.0055	1	No gap

$z_3 (> z_2)$, which causes the Te(1) layers between neighboring QLs to interact via weak van der Waals forces, allowing exfoliation [17]. For the slab electronic structure, we use VASP [26] with the PBE GGA and PAW pseudopotentials as in the bulk case. We do not perform reconstruction of the surfaces. Compared to the bulk case, the electronic structure of the slabs, especially of surface bands, converges more slowly with parameter values (E_c , N_k , and the number of vacuum layers). For the six slabs with different thicknesses considered, a large vacuum layer equivalent to 5 QLs (=50.829 Å) is added. The values of E_c and N_k used for the six slabs are listed in Table I.

Self-consistent DFT calculations with SOC are first carried out using the parameter values listed in Table I until the total energy converges to within 1×10^{-6} eV. The two-dimensional band structure is then computed non-self-consistently using a charge density distribution obtained from the previous self-consistent calculations. Accuracy in the structure of the surface bands depends on the accuracy in the charge density distribution. Thus, extremely well-converged self-consistent calculations are required for an accurate identification of the surface bands.

We now introduce our method to identify surface states from the slab band structure. Surface bands refer to bands localized on the top or bottom surface layers of a slab [29], but not all bands in a slab belong to the sur-

face bands. To identify surface bands, a wave function at a given energy band and \bar{k}_{\parallel} (momentum parallel to the surface) is projected onto spherical harmonics which are non-zero within some radius around each ion. Then two criteria are applied to the wave function projections. In criterion 1, the surface bands are identified based on a critical percentage of the projections onto the top two or the bottom two atomic layers. The critical percentage depends on the slab thickness. In criterion 2, the surface bands are identified according to a critical percentage of the projections onto the top or the bottom QL. Criterion 2 is suitable for multiple QLs. The density of states (DOS) projected onto each atomic layer of the topmost and bottommost QL reveals that the DOS projected onto the inner Te(1) layers more closely resembles that projected onto the outer Te(1) layers than those onto the middle Te(2) layers [inset in Fig. 2(b)]. Additionally, the electron density spreads over all five atomic layers within the topmost or bottommost QL.

Band structures of $\text{Bi}_2\text{Te}_3(111)$ slabs of 1-6 QLs, are shown in Fig. 2 with the surface bands marked. Here the surface bands are identified by applying criterion 1 to the 1 QL and 2 QL slabs and criterion 2 to the other slabs. Critical percentages are self-consistently determined such that the wave function projections onto the surfaces are stable. The specific critical percentages are as follows: 45% and 30% for 1 QL and 2 QLs, respectively, and 60%, 50%, 40%, and 40% for 3 QLs, 4 QLs, 5 QLs, and 6 QLs, respectively. For very thin slabs (1-2 QLs), criterion 2 is not applied. When criterion 1 is applied to the slabs thicker than 2 QLs, the critical percentages are 25%, 20%, 16%, and 16% for 3 QLs, 4 QLs, 5 QLs, and 6 QLs, respectively. Among the surface states marked in Fig. 2, only those within 0.2 eV above and 0.3 eV below E_f near $\bar{\Gamma}$ survive as surface states. The surface bands outside this energy window, far away from $\bar{\Gamma}$, are strongly coupled to the bulk bands [Fig. 1(b)]. A comparison of the surface bands identified using the criteria 1 and 2 reveals that the surface states within the energy window remain essentially unchanged using the different criteria.

Now we present a physical interpretation of the surface states identified above. Let us first consider a very thick slab where the top surface bands do not interact with the bottom surface bands. When the thick slab has symmetric surfaces (the top and bottom surfaces in an identical environment), the surface bands become fourfold degenerate at $\bar{\Gamma}$, because of Kramers degeneracy at the time-reversal invariant momentum for both the top and bottom surfaces. Away from $\bar{\Gamma}$, the fourfold degeneracy is lifted to a twofold degeneracy due to SOC. Neglecting the fact that the spin-up and spin-down states are not eigenstates in the presence of SOC, for a symmetric thick slab, the top surface bands with spin-up (spin-down) are degenerate with the bottom surface bands with spin-down (spin-up).

As the slab thickness decreases, the top surface bands

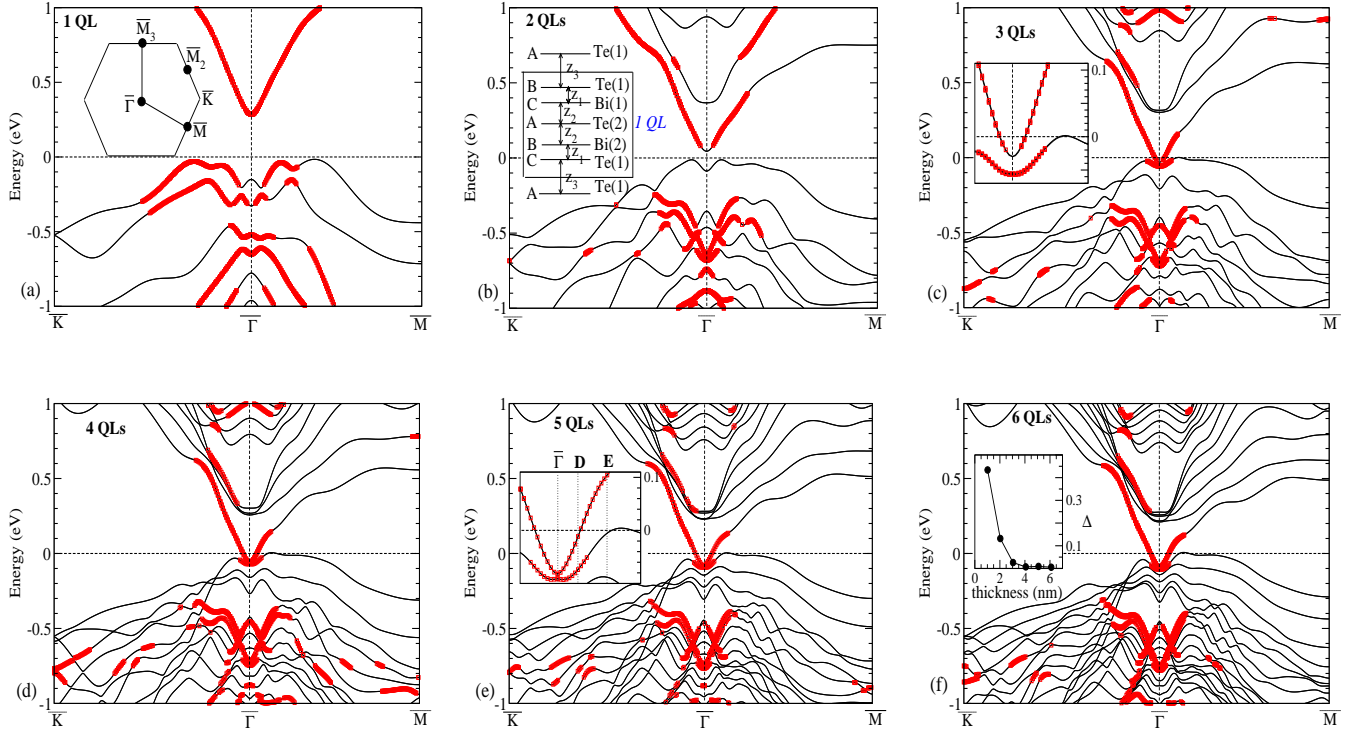


FIG. 2: (Color online) Band structures of $\text{Bi}_2\text{Te}_3(111)$ films with six thicknesses (surface states marked by the squares). Inset in (a): Two-dimensional Brillouin zone. Inset in (b): Schematic view of one QL of a $\text{Bi}_2\text{Te}_3(111)$ film. A, B, and C indicate the planar sites of the Te and Bi atoms. $z_1=1.737 \text{ \AA}$, $z_2=2.033 \text{ \AA}$, $z_3=2.625 \text{ \AA}$ [25]. Inset in (c): Zoom-in of the 3 QL band structure near $E_f = 0$. Inset in (e): Zoom-in of the 5 QL band structure near $E_f = 0$. Inset in (f): Δ (eV) vs thickness (nm).

TABLE II: Wave function projections onto each QL (from the topmost to the bottommost QL) for the 5 QL slab, as a function of energy band and k_{\parallel} . The specific k_{\parallel} points for the V-shaped (U-shaped) band shown in the inset of Fig. 2(e) are labeled as $\bar{\Gamma}_V$, D_V , E_V ($\bar{\Gamma}_U$, D_U , E_U). Each band has a double degeneracy. Two wave functions corresponding to $\bar{\Gamma}_V$ have the following projections onto each QL with the opposite spin moments: (0.503,0.204,0.024,0.085,0.189), (0.189,0.085,0.024,0.204,0.503). The surface states (SS) are identified based on the criterion 2.

	$\bar{\Gamma}_U$	$\bar{\Gamma}_V$	D_U	D_V	E_U	E_V
k_{\parallel} ($2\pi/a$)	0	0	0.022	0.022	0.057	0.057
Energy(eV)	-0.091	-0.082	-0.074	-0.012	-0.001	0.111
topmost	0.438	0.503	0.490	0.795	0.328	0.573
top-1	0.190	0.204	0.356	0.182	0.323	0.274
middle	0.060	0.024	0.128	0.016	0.187	0.101
bottom+1	0.094	0.085	0.023	0.000	0.083	0.038
bottommost	0.217	0.189	0.003	0.000	0.080	0.017
SS?	Yes	Yes	Yes	Yes	No	Yes

interact with the bottom surface bands, resulting in an opening of a band gap Δ , even at $\bar{\Gamma}$. At $\bar{\Gamma}$, a linear even combination of the top spin-up and the bottom spin-up

surface states are degenerate with a linear even combination of the top spin-down and the bottom spin-down surface states. At $\bar{\Gamma}$, the energies of these even combinations are separated from those of the similar odd combinations (with a double degeneracy) by Δ . This gap increases with increasing k_{\parallel} . As the thickness decreases, Δ increases. Even though the symmetric slab still possesses time-reversal and inversion symmetry, a strong interaction between the top and bottom surfaces mixes spin-up with spin-down states, resulting in a reduction in spin polarization at each surface. Thus, spin-flip scattering at each surface will no longer be suppressed. However, the thin slab must show a remnant of a bulk TI: the number of E_f crossings of the surface bands for a given surface (either the top or bottom surface).

Our calculated values of Δ at $\bar{\Gamma}$ and of the indirect band gap ΔE_{ind} corroborate robust surface states for three or more QLs. The 1 QL and 2 QL slabs show Δ of 0.4338 and 0.1319 eV at $\bar{\Gamma}$, respectively. This gap decreases exponentially with increasing thickness and it saturates at a thickness of 4 QLs [Table I, inset in Fig. 2(f)], in agreement with Refs. [19, 21]. For the slabs four or less QLs thick, Δ does not originate entirely from the surface states. At $\bar{\Gamma}$, for the slabs three or less QLs thick, the valence band does not have a surface character [Fig. 2(a),(b), the V-shaped band in the inset of

(c)], while for the 4 QL slab, the band slightly below the V-shaped band loses its surface character. However, as k_{\parallel} increases, for the 3 QL (4 QL) slab, the V-shaped band (the band slightly below the V-shaped band) retrieves its surface character. The 1 QL and 2 QL slabs show ΔE_{ind} of 0.301 and 0.057 eV, respectively. As the thickness increases, ΔE_{ind} vanishes.

We now use our accurate identification of surface states in the slabs to examine their topological properties. For a three-dimensional TI, ν_0 is determined from the bulk band structure by a product of parity eigenvalues of all occupied bands (counting Kramers degenerate pairs only once) at the eight time-reversal invariant momenta [1]. However, this procedure is not well defined in slabs. Thus, instead, we use an equivalent criterion [1]. The surface bands of a TI cross E_f an odd number of times between time-reversal invariant momenta ($\nu_0 = 1$). With the notations in Ref.[1], ν_0 can be obtained from $(-1)^{\nu_0} = \pi_{\bar{\Gamma}}\pi_{\bar{M}}\pi_{\bar{M}_2}\pi_{\bar{M}_3}$, where $\bar{\Gamma}$, \bar{M} , \bar{M}_2 , and \bar{M}_3 are four time-reversal invariant momenta in the two-dimensional Brillouin zone [inset in Fig. 2(a)]. If the surface bands cross E_f an odd (even) number of times between $\bar{\Gamma}$ and \bar{M} , then $\pi_{\bar{\Gamma}}\pi_{\bar{M}} = -1$ (+1). Another equivalent criterion states that the conduction and valence bands with opposite parities are inverted by SOC at the Dirac point ($\bar{\Gamma}$) for slabs with topologically non-trivial surface states. These two criteria must provide the same result.

For the 1 QL and 2 QL slabs, the surface states neither cross E_f between $\bar{\Gamma}$ and \bar{M} [Fig. 2(a),(b)] nor between \bar{M}_2 and \bar{M}_3 . Thus, the 1 QL and 2 QL slabs have topologically trivial ($\nu_0 = 0$) surface states. This is also corroborated by our finding that the conduction and valence bands are not inverted at $\bar{\Gamma}$ by SOC. Note that the topologically trivial nature of the surface states would not change by shifting E_f upward.

Let us discuss the slabs three or more QLs thick. Their surface states are marked in Fig. 2(c)-(f). Within the small energy window from E_f , only two surface bands are identified. The features of these two surface bands discussed below do not depend on the thickness. To better examine the surface states, for example, for the 5 QL slab, the projections of the wave function onto each QL at three k_{\parallel} -points for the two energy bands [shown in the inset of Fig. 2(e)] are listed in Table II. The V-shaped valence band near $\bar{\Gamma}$ is a surface band [Fig. 2(c)-(f)]. This surface band intersects E_f only once between $\bar{\Gamma}$ and \bar{M} [insets in Fig. 2(c),(e)] and joins the bulk bands as k_{\parallel} moves further away from $\bar{\Gamma}$. The occupied U-shaped band slightly below the V-shaped band near $\bar{\Gamma}$ [insets in Fig. 2(c),(e)], is again a surface band only within a very narrow window in k_{\parallel} , yet it loses its surface character before it crosses E_f [see the projections of this band at the E point, E_U , in Table II and the inset of Fig. 2(e)]. Additionally, none of the surface bands cross E_f between

\bar{M}_2 and \bar{M}_3 . SOC indeed inverts the conduction and valence bands. Thus, *slabs three or more QLs thick have topologically non-trivial ($\nu_0=1$) surface states, independent of the thickness*. Our findings clearly reveal that the topological nature of the surface states persists with the thickness, differing from previous calculations [21], yet in agreement with experiment [19].

We have constructed a method to accurately identify topological surface states within DFT. Using this method, we have investigated the topological nature of the surface states in thin films of Bi₂Te₃(111) using DFT. We have found that the topological nature of the surface states remains robust with the film thickness and that the surface states are topologically protected for films of three or more QLs. The method and our findings are applicable to thin films of other types of TI.

The authors thank T. Stanescu for discussions. K.P. was supported by NSF DMR-0804665, D.M. by US DOE DE-FG05-92ER40677, J.J.H. by US DOE DE-FG02-08ER46532. Computational support was provided by Intel 64 cluster (Abe) at the NCSA under DMR060009N and VT ARC.

-
- [1] L. Fu and C. L. Kane, Phys. Rev. B **76**, 045302 (2007).
 - [2] J. C. Teo *et al.*, Phys. Rev. B **78**, 045426 (2008).
 - [3] X.-L. Qi *et al.*, Phys. Rev. B **78**, 195424 (2008).
 - [4] M. Z. Hasan and C. L. Kane, arXiv:1002.3895v1.
 - [5] H. Zhang *et al.*, Nat. Phys. **5**, 438 (2009).
 - [6] D. Hsieh *et al.*, Nature **452**, 970 (2008); D. Hsieh *et al.*, Science **323**, 919 (2009).
 - [7] Y. L. Chen *et al.*, Science **325**, 178 (2009).
 - [8] D. Hsieh *et al.*, Phys. Rev. Lett. **103**, 146401 (2009).
 - [9] Y. Xia *et al.*, Nat. Phys. **5**, 398 (2009).
 - [10] D. Hsieh *et al.*, Nature **460**, 1101 (2009).
 - [11] T. Zhang *et al.*, Phys. Rev. Lett. **103**, 266803 (2009).
 - [12] P. Roushan *et al.*, Nature **460**, 1106 (2009).
 - [13] K. K. Gomes *et al.*, arXiv:0909.0921.
 - [14] W. Zhang *et al.*, arXiv:1003.5082.
 - [15] P. Ghaemi *et al.*, arXiv:1002.1341v1.
 - [16] G. Zhang *et al.*, Appl. Phys. Lett. **95**, 053114 (2009).
 - [17] D. Teweldebrhan *et al.*, Appl. Phys. Lett. **96**, 053107 (2010).
 - [18] Y. Zhang *et al.*, arXiv: 0911.3706.
 - [19] Y.-Y. Li *et al.*, arXiv:0912.5054.
 - [20] Y. Sakamoto *et al.*, Phys. Rev. B **81**, 165432 (2010).
 - [21] C.-X. Liu *et al.*, Phys. Rev. B **81**, 041307 (R) (2010).
 - [22] J. Linder *et al.*, Phys. Rev. B **80**, 205410 (2009).
 - [23] H.-Z. Lu *et al.*, Phys. Rev. B **81**, 115407 (2010).
 - [24] S. K. Mishra *et al.*, J. Phys.: Cond. Mat. **9**, 461 (1997).
 - [25] S. Nakajima, J. Phys. Chem. Solids. **24**, 479 (1963).
 - [26] G. Kresse and J. Furthmüller, Phys. Rev. B **54**, 11169 (1996); G. Kresse and J. Furthmüller, Comp. Mat. Sci. **6**, 15 (1996).
 - [27] J. P. Perdew *et al.*, Phys. Rev. Lett. **77**, 3865 (1996).
 - [28] P. E. Blöchl, Phys. Rev. B **50**, 17953 (1994).
 - [29] J. Furthmüller *et al.*, Phys. Rev. B **53**, 7334 (1996).